Appendix C

Supporting Information for

Chapter 5: Manganese Oxidation Induced by Water Table Fluctuations in a Sand Column.

Contents: 6 figures and 9 tables

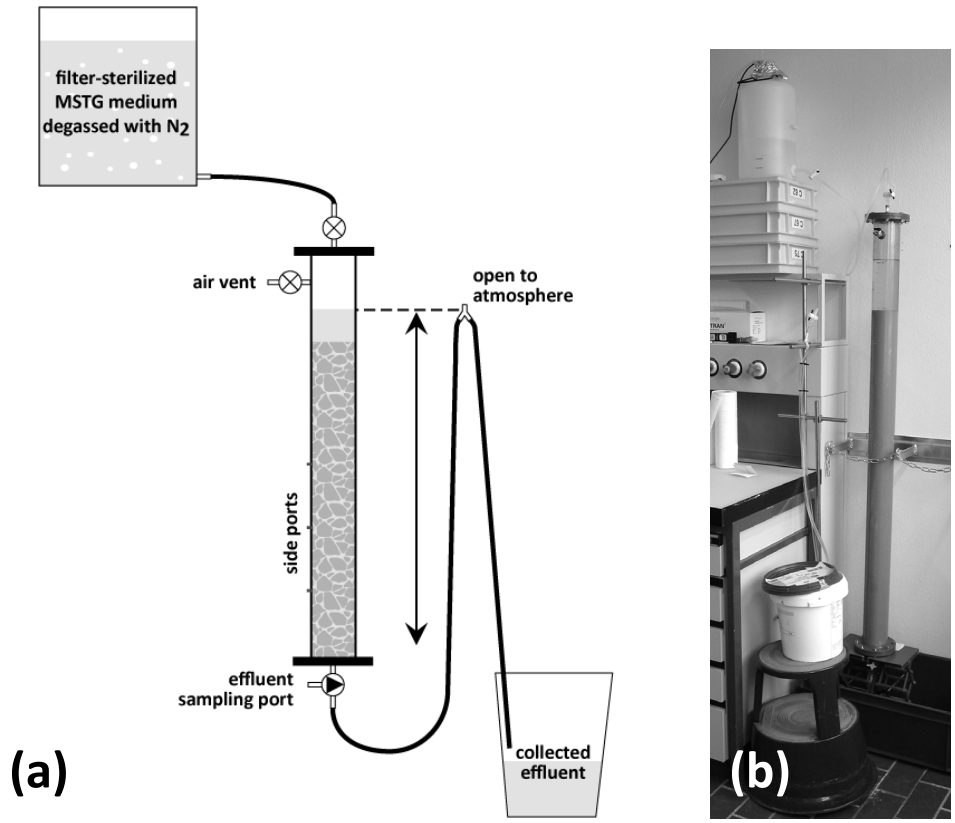

Figure C.1. Schematic (not to scale, a) and photo (b) of the column setup.

Table C.1. Results of oxidation assays at the end of the column experiment

sample #		OD_{600} t = 34 h	% Mn(II)	% Mn oxide
1	fresh MSTG, no cells	0.0529	100	0
2	fresh +plate, -Zn	0.1948	1	99
3a	fresh +effluent, -Zn	0.1948	1	99
3b	fresh +effluent, +Zn	0.3083	100	0
4	influent (+Zn)	0.3532	79	21

The first four batches used freshly prepared and filter-sterilized MSTG medium: (1) without inoculation, (2) inoculated from a plated GB-1 cell culture, and (3a) inoculated with the effluent at the end of the column experiment. One effluent-inoculated batch (3b) also contained 15 μM $ZnCl_2$. In addition, one batch used the column influent solution (4), which contained 15 μM $ZnCl_2$, collected at the end of the column experiment without deliberate inoculation; since that solution should have been sterile, some contamination

of the influent with cells able to travel upward along the column walls and through the 0.45 μm filter was suspected.

Lack of growth and oxidation in the fresh MSTG without cells (sample 1) confirms that the MSTG preparation was sterile. Remarkably, the OD_{600} and % oxidation were identical for the Zn-free batches inoculated with column effluent (3a) and directly from the refrigerated LB agar plate (2). Although no replicate assays were performed, this suggests strong similarity between the plated culture and the active culture in the column. The addition of Zn to a batch inoculated with column effluent (3b) resulted in complete inhibition of Mn oxidation, despite a slight growth enhancement. Intriguingly, the cells in the influent that included Zn (4) were able to grow even more and oxidized a fraction of the total Mn (N_2 degassing inhibited cell growth in the influent during the column experiment). This suggests that the pure culture eventually adjusted somewhat to the presence of Zn, or that a mixed culture developed inside the influent reservoir. On the other hand, this batch did not contain visible Mn oxides (+Zn batches had a greenish hue), so it is perhaps more likely that the nonzero Mn oxide fraction in this batch is an artifact of the extraction technique. Even if the column contained a mixed culture, the oxidation of significant amounts of Mn(II) during water table fluctuations does not detract from the end result of the paper.

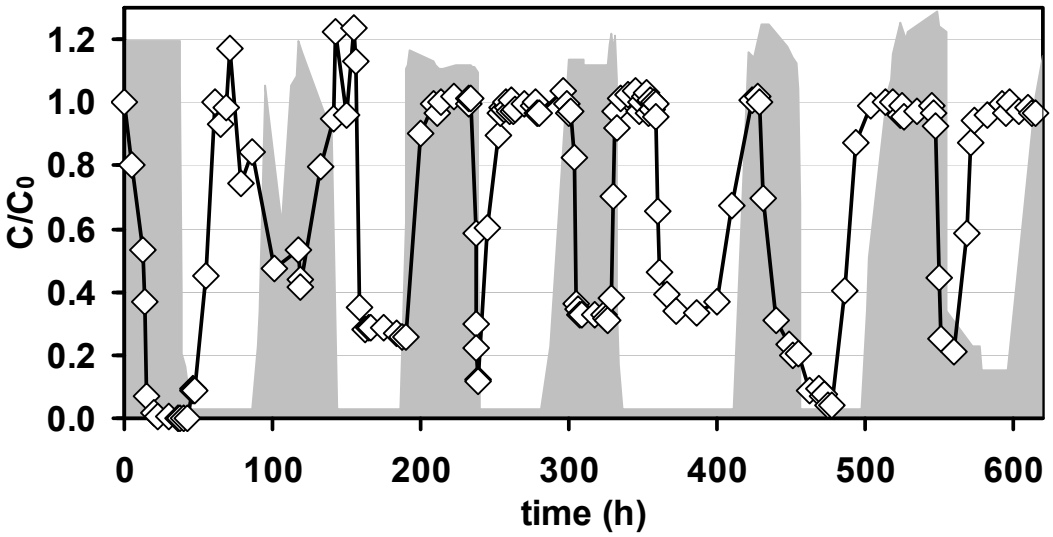

Figure C.2. Filtered relative effluent concentrations of Br (◇, C_0 = 10 μM). For reference, the water level in the column is shown in the shaded profile (note the vertical scale is different than Figure 5.1). Variation in Br derives from concentration differences in alternate batches of influent solution ("pulsed" inlet concentration). Up to 150 h, preferential flow paths and leaks through the column's side ports resulted in non-ideal flow behavior. Between concentration pulses, C/C_0 does not always approach 0 because 5-l batches of Br-free MSTG were added to the residual Br-containing MSTG in the influent reservoir, which was always > 0.5 l due to reservoir geometry.

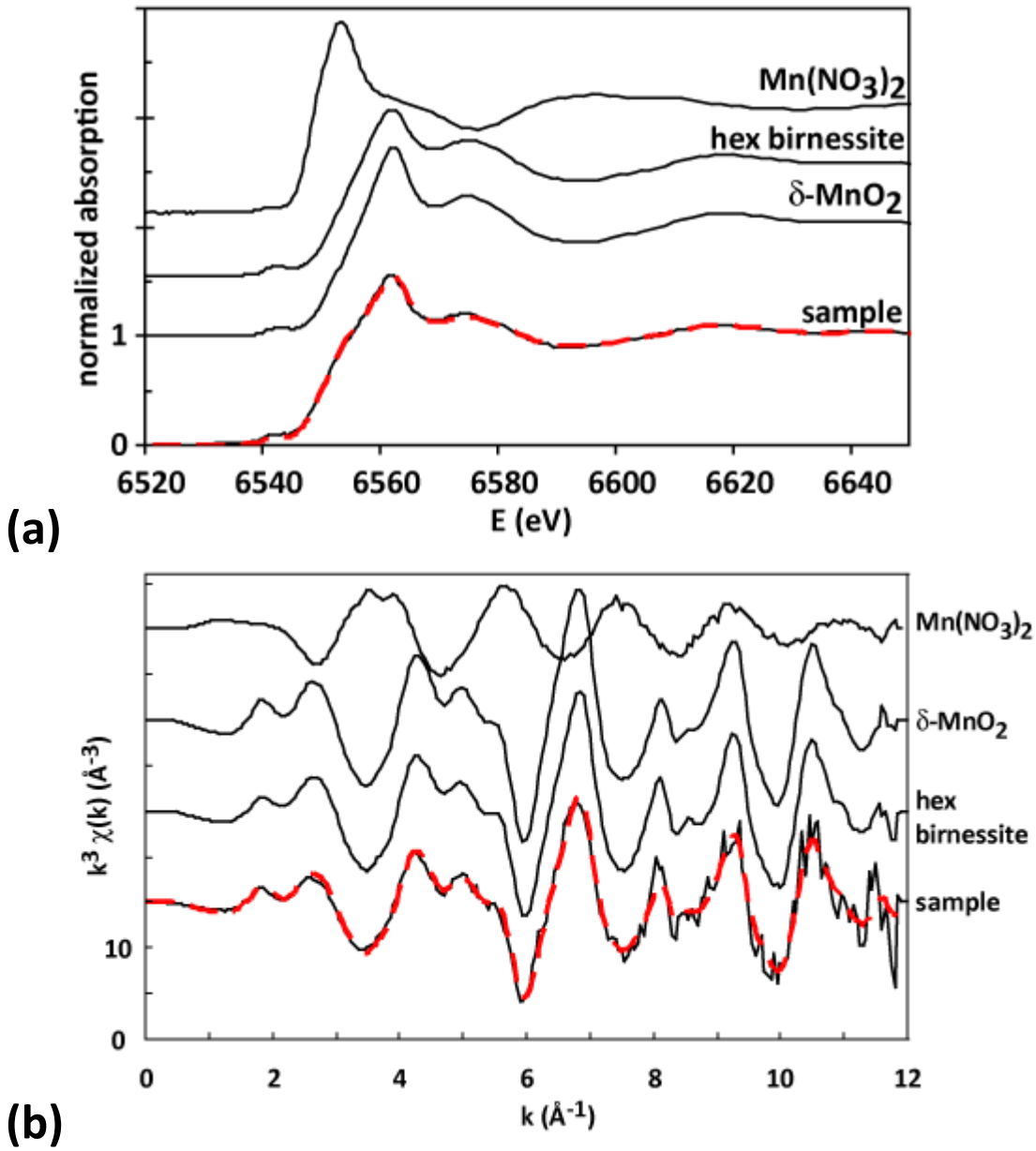

Figure C.3: (a) XANES and (b) EXAFS spectra of Mn at the top of the sand column, compared to linear combination fit (LCF) spectra based on reference spectra for aqueous Mn^{2+}, δ-MnO_2 (Webb et al. 2005), and hexagonal birnessite (Webb et al. 2005). LCF parameters are provided in Table C.2.

Comparison of the sample spectrum to the spectra of δ-MnO_2 (Mn oxidation state 3.8 (Villalobos et al. 2003)) and aqueous Mn^{2+} clearly indicates the presence of some Mn(II) in the sample spectrum. This Mn(II) fraction likely accounts for Mn^{2+} adsorbed to or inside bacteria, or sorbed to the Mn-precipitate or sand. Based on the LCF results for the

XANES region (considered more sensitive and reliable than the EXAFS region to quantify the Mn(II) fraction), this Mn(II) fraction was estimated to account for about 20% of the total Mn in the sand sample. Regarding the type of Mn oxide, the features in the EXAFS at 8 and 9.3 $Å^{-1}$ were characteristic for the phyllomanganates δ-MnO_2 and hexagonal birnessite but clearly distinct from the EXAFS of triclinic birnessite or the tectomanganate todorokite (Webb et al. 2005). This was confirmed by LCF analysis, which showed that the sample EXAFS spectrum could be reasonably reproduced by a combination of δ-MnO_2 and hexagonal birnessite.

Table C.2: Linear combination fit results for Mn XANES and EXAFS spectra at the top of the sand column

	δ-MnO_2	**hexagonal birnessite**	**aqueous Mn^{2+}**	**sum**	**NSSR[a]**
XANES	0.53 (0.04)[b]	0.28 (0.04)	0.20 (0.00)	1.01	4.6×10^{-4}
EXAFS	0.53 (0.13)	0.30 (0.14)	0.07 (0.00)	0.91	4.5×10^{-2}

[a]normalized sum of squared residuals = $\sum(data_i\text{-}fit_i)^2/\sum data_i^2$
[b]values in parentheses indicate fit uncertainty

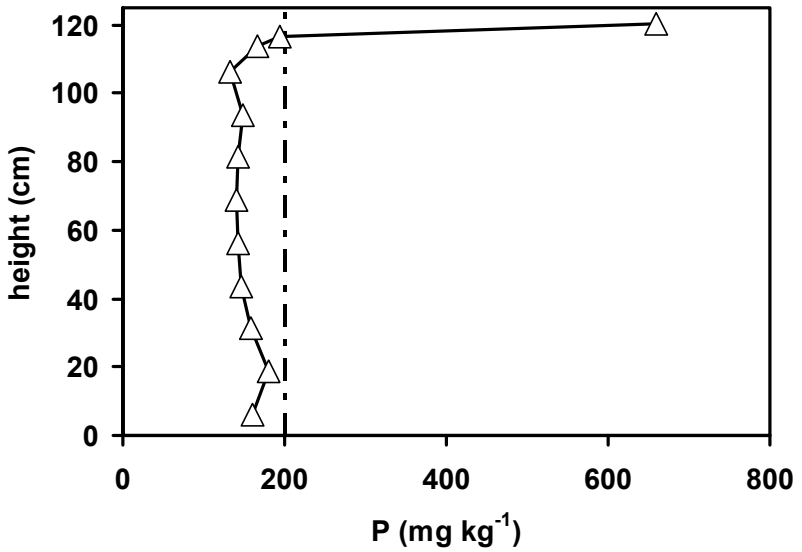

Figure C.4. XRF profile of P along the column at the end of the experiment. Dashed line indicates the background of unused sand. Other measured elements had no significant trend with height (not shown). Of note, the Fe concentration was below detection (1 mg kg^{-1}) in all samples.

Table C.3. Pseudo-first-order rate coefficients for Mn oxide reduction and OD_{600} during the reduction assay (averages of 3 replicate batches)

	k′ (h^{-1})	**OD_{600} t = 15 h**	**OD_{600} t = 64 h**
blank: MSTG only	0.0030 ± 0.0015	0.0531	0.0396
exponential: MSTG + *P. putida* GB-1[a]	0.0047 ± 0.0012	0.4328	0.2037
stationary: MSTG + *P. putida* GB-1[b]	0.0041 ± 0.0022	0.4441	0.2125

[a] Mn-doped gels were added at the beginning of exponential phase.
[b] Mn-doped gels were added at the beginning of stationary phase.

The rates for the two types of *P. putida* batches were not significantly different. Relatively large standard deviations for k′ (up to 50%) reflect the low amounts of Mn lost from the gels relative to the variation between individual gels. OD_{600} for the blank likely decreased due to colloidal components diffusing into the gels. The difference in OD_{600} at 15 h for exponential and stationary batches suggests a small inhibition of cell growth by the polyacrylamide gels doped with hydrous Mn oxide.

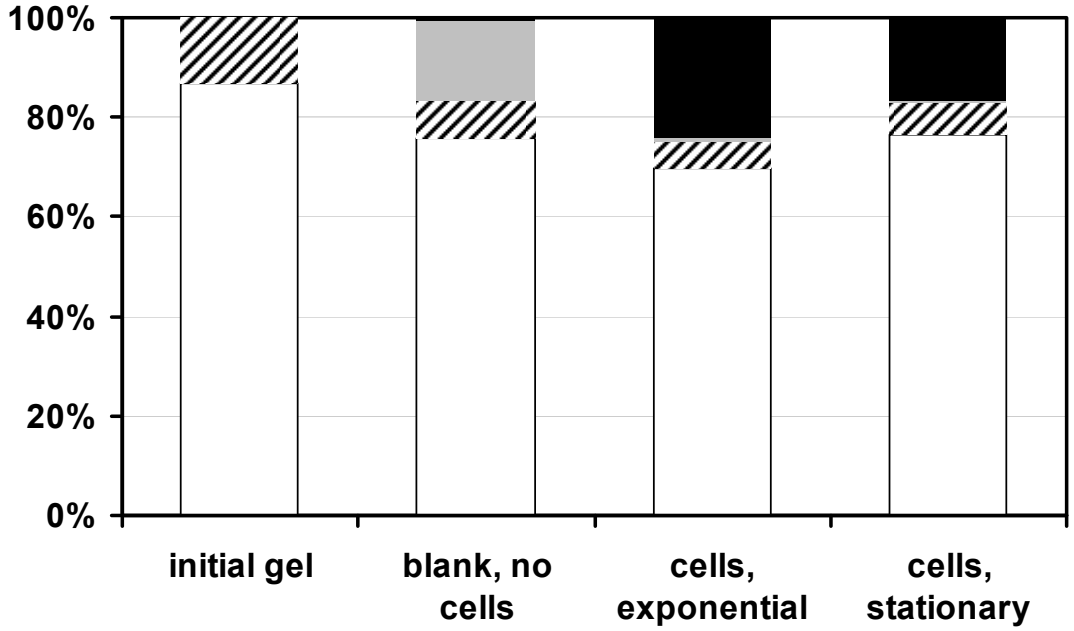

Figure C.5. Mass balance for unreacted gels ("initial gel") and batches at the end of the reduction assays (three replicates each), given as % of total mol Mn per batch. The white bar represents Mn oxide remaining in the gel, the striped bar represents Mn(II) remaining in the gel, the grey bar represents Mn(II) in solution, and the black bar represents Mn oxide in solution. Mn(II) was extracted with 0.05 M $Cu(NO_3)_2$ in 0.05 M $Ca(NO_3)_2$, while Mn oxide was calculated from the hydroxylamine-HCl-extracted total Mn minus the Mn(II). Total mass balance for each set of batches was closed within 4%. In the absence of cells, MSTG medium oxidized 4% of the solution-phase Mn (0.7% of the total Mn) in 64 h, which is negligible.

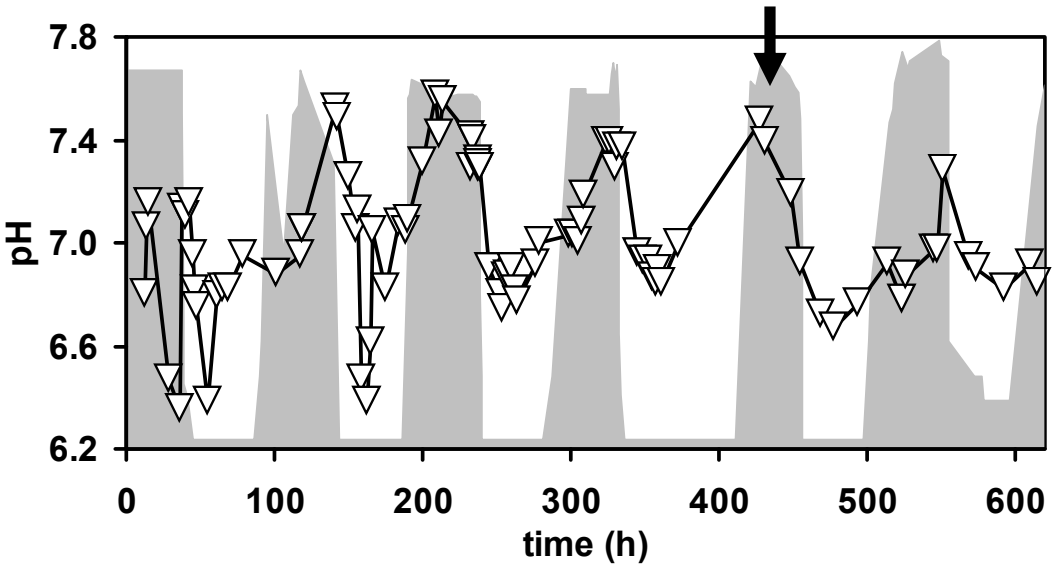

Figure C.6. Effluent pH (▽, influent pH = 7.5) measured directly at the base of the column. The arrow denotes the addition of 15 μM Zn to the influent. For reference, the water level in the column is shown in the shaded profile (note the vertical scale is different than Figure 5.1a). Low values in pH (< 6.6) before 60 h may indicate washout of residual amounts of Nanopure water (pH 5.5) trapped in the pore spaces.

Details of Mn Oxidation Rate Calculations

Abiotic Mn oxidation rate expressions are well-established in the literature.

Homogeneous Mn oxidation rate has been expressed (Morgan 2000):

$$-\frac{d[Mn^{2+}]}{dt} = k_1[O_2][OH^-]^2[Mn^{2+}] = k[Mn^{2+}] \qquad \text{(C-1)}$$

where k_1 is approximately 2×10^{12} M^{-3} d^{-1}, and k represents the pseudo-first-order rate constant. Heterogeneous Mn oxidation in this system is dependent on two different surfaces for catalysis: Mn oxides, here represented as MnO_2, and quartz sand, here represented as SiO_2. Mn adsorption to both surfaces has a reported (Davies and Morgan 1989) half-life of 5 min, so oxidation is assumed to be the only relevant step in the oxidation rate. Surface catalysis by Mn oxides was studied using hydrous Mn oxide (δ-

MnO_2) (Morgan and Stumm 1964), which is a high-surface-area analog of natural biogenic Mn oxides (Villalobos et al. 2003). Its ability to catalyze Mn oxidation has been expressed (Morgan 2000):

$$-\frac{d[Mn^{2+}]}{dt} = k_{Mn}[O_2][OH^-]^2[MnO_2][Mn^{2+}] = k_s[MnO_2][Mn^{2+}] \quad \text{(C-2)}$$

where k_{Mn} is approximately 5×10^{12} M^{-4} d^{-1}. The surface area and reactivity of δ-MnO_2 are assumed to be approximately equivalent to that of the Mn oxides in the column. Surface catalysis by SiO_2 was studied with nanoparticulate silica (Davies and Morgan 1989), a significantly different material than quartz sand. The rate expression for SiO_2-catalyzed Mn oxidation is:

$$-\frac{d[Mn^{2+}]}{dt} = k''a\{(>SO)_2Mn\}pO_2 = k''a\,{}^*\beta_2^s\{SOH\}[Mn^{2+}][H^+]^{-2}\,pO_2 \quad \text{(C-3)}$$

where k″ is 0.01 min^{-1} atm^{-1}, a is the mass loading (g l^{-1}), ${}^*\beta_2^s$ is $10^{-13.9}$ M, and {SOH} is 0.0015 mol g^{-1}, following Davies and Morgan (Davies and Morgan 1989). The surface area of nanoparticulate silica (182 m^2 g^{-1}) is orders of magnitude larger than that of the quartz sand, which was estimated to be 9.4×10^{-3} m^2 g^{-1} based on spherical particles with a diameter of 0.24 mm and a density of 2.65 g cm^{-3} (the surface area was too low to be measured by BET). The reactive surface sites and bidentate surface complexes are assumed to be the same for the two solids, and the reactivity is assumed to be proportional to the surface area. Thus, the rate constant k″ was scaled to the surface area of the quartz sand in the column.

To calculate the abiotic oxidation rates at the conditions inside the column, dissolved oxygen in equilibrium with air (or in the case of equation (C-3), pO_2 was 0.21 atm) and pH 7 were assumed. The maximum effluent dissolved oxygen was only 42%

saturation (Figure 5.2) and influent DO was always < 10%, so the calculated rates are faster than expected for the column's conditions. Although pH fluctuated between 6.35 and 7.55 (Figure C.6), the average was 7.01. The molar concentration of MnO_2 in equation (C-2) was estimated with the average XRF concentration across the column at the end of the experiment (20.5 mg kg^{-1}), the mass of Mn, and the mass of sand (~ 10 kg) in the column volume (~ 6 l). The mass of sand per liter was also used as "a" in equation (C-3). Finally, the influent [Mn^{2+}] of 100 μM was used in all three equations and the units converted to μM h^{-1}.

Table C.4. Observed levels of water table (WT; measured as cm above the base of the column) during experiment

time (h)	WT
0	135.5
4.63	135.5
12.75	135.5
13.50	135.5
14.50	135.5
16.92	135.5
20.58	135.5
22.50	135.5
29.25	135.5
36.17	135.5
37.50	135.5
37.67	123.9
38.67	65
39.50	48
41.25	44.5
45.33	32.5
46.60	32.5
47.83	32.5
54.60	32.5
61.33	32.5
65.33	32.5
69.33	32.5
71.83	32.5
79.30	32.5
86.75	32.5
89.17	50
90.67	60
94.17	121
94.83	123.5
106.83	84.5
111.58	123.5
115.33	126
117.58	135.5
119.00	132.5
139.58	110
142.58	32.5
150.00	32.5
155.17	32.5
156.75	32.5
159.33	32.5
162.67	32.5
164.50	32.5
166.33	32.5
175.25	32.5
184.16	32.5
185.08	32.5
188.58	85
189.83	128
190.24	128.7
191.21	133.2
207.96	130
208.41	129
211.08	128
213.75	128
222.92	129
232.08	129
233.08	128.5
234.08	128.5
237.50	127
237.67	100
237.83	73
238.00	50
238.50	32.5
239.00	32.5
252.17	32.5
254.67	32.5
259.50	32.5
262.17	32.5
263.17	32.5
276.67	32.5
279.08	32.5
285	50
298.17	130.4
301.83	130.4
304.67	130.4
307.42	130.4
308.67	129
323.67	129
325.50	134.5
326.75	137.5
327.92	133.5
329.08	136.5
329.83	137.3
330.54	125
330.70	95
330.92	62
331.08	45
334.83	32.5
345.25	32.5
348.92	32.5
352.75	32.5
355	32.5
357.58	32.5
359.08	32.5
360.83	32.5
372.33	32.5
399.5	32.5
408.08	32.5
418.58	132.5
421.20	130.8
426.92	140.3
431.58	140.1
444.33	134
448.83	130.8
450.21	129.4
451.83	122
452	90
452.2	50
453.58	32.5
454.5	32.5
469.25	32.5
472.5	32.5
477.75	32.5
494.33	32.5
497.67	60
498.67	75
511.83	121
513.33	125
515	132
519.67	140.6
523.58	136
525.75	138.2
544.58	144
544.83	144
546.83	140
550	138.2
550.17	135.5
550.38	130.4
550.52	128
550.92	100
551.33	75
551.7	60
568.58	50
569.08	50
573.83	50
574.67	43.3
590	43.3
592.16	43.3
610.5	120
615.25	131.3

Table C.5. Dissolved oxygen concentrations in the column effluent

time (h)	DO%	mg/L
0.00	1.5	0.13
37.50	5.8	0.47
39.50	9	0.7
45.33	21.3	1.81
47.83	24	2.05
61.33	27.1	2.32
69.33	19.2	1.65
71.83	23.9	2.05
86.75	25	2.14
118.25	5	0.43
119.00	3.3	0.28
141.83	14	1.20
142.33	16.3	1.40
155.17	34.3	2.94
156.25	35.6	3.05
159.33	36	3.08
162.67	36	3.08
166.33	37.9	3.26
184.16	36	3.09
187.30	1.5	0.13
190.41	2.1	0.18
208.41	1.6	0.14
213.75	1.4	0.12
232.08	1.6	0.14
234.08	12.5	1.07
237.33	8.6	0.73
237.67	13.3	1.13
238.00	16.4	1.40
238.50	14.8	1.26
239.00	15	1.28
252.17	18.7	1.61
257.83	29.6	2.54
259.50	24.5	2.10
262.17	27.8	2.38
263.17	30.6	2.61
276.67	32.3	2.76
279.08	23.3	2.00
298.42	12	1.02
301.83	2.3	0.20
304.67	3.2	0.27
307.42	2.3	0.20
308.67	2	0.17
323.67	9.1	0.78
326.75	15.5	1.33
329.92	9.8	0.83
331	14.1	1.19
334.83	16.1	1.38
345.25	34.7	2.97
348.92	36.1	3.09
352.75	41.7	3.56
355	36.6	3.13
357.58	40	3.42
359.08	35.7	3.05
360.83	39.2	3.35
372.33	38.5	3.30
399.5	32.9	2.82
426.92	16.3	1.39
431.58	12.6	1.08
448.83	10.6	0.90
454.5	33.1	2.82
469.25	33.5	2.88
472.5	37.7	3.22
477.75	30.3	2.59
494.33	32.9	2.81
513.33	2.2	0.19
523.58	2.1	0.18
525.75	2.7	0.23
544.83	11.6	0.99
547.9	12.3	1.05
551.4	19.8	1.68
569.08	34.1	2.92
573.83	31.4	2.69
592.16	24	2.05
610.5	14.5	1.24
615.25	13.2	1.12

Table C.6. pH values in the column effluent

time (h)	pH
12.75	6.80
13.50	7.06
14.50	7.15
29.25	6.47
36.17	6.35
37.50	7.13
39.50	7.10
42.50	7.15
45.33	6.95
46.60	6.81
47.83	6.75
54.60	6.38
61.33	6.79
65.33	6.82
69.33	6.82
79.30	6.95
100.83	6.88
117.92	6.95
118.25	7.05
119.00	7.05
141.83	7.52
142.33	7.48
150.00	7.25
155.17	7.05
156.75	7.12
159.33	6.47
162.67	6.38
164.50	6.61
166.33	7.04
175.25	6.82
184.16	7.07
188.30	7.04
190.41	7.09
199.41	7.31
208.41	7.57
211.08	7.42
213.75	7.55
232.08	7.41
233.08	7.29
234.08	7.40
237.33	7.32
237.67	7.30
238.00	7.29
238.50	7.29
239.00	7.29
245.60	6.90
252.17	6.80
253.40	6.74
256.25	6.86
257.83	6.87
259.50	6.90
262.17	6.81
263.17	6.77
276.67	6.91
279.08	7.00
298.42	7.03
301.83	7.03
304.67	7.00
307.42	7.08
308.67	7.18
323.67	7.39
326.75	7.39
329.92	7.29
331	7.37
334.83	7.37
345.25	6.96
348.92	6.93
352.75	6.93
355	6.86
357.58	6.84
359.08	6.89
360.83	6.84
372.33	6.99
426.92	7.47
431.58	7.39
448.83	7.19
454.5	6.92
469.25	6.72
477.75	6.67
494.33	6.76
513.33	6.92
523.58	6.78
525.75	6.87
544.83	6.97
547.9	6.97
551.4	7.28
569.08	6.94
573.83	6.90
592.16	6.82
610.5	6.91
615.25	6.84

Table C.7. Mn C/C_0 values in the column effluent

time (h)	C/C_0	time (h)	C/C_0	time (h)	C/C_0	time (h)	C/C_0
13.5	0.00	237.67	0.94	356.29	0.00	597.75	0.07
14.5	0.00	238	0.93	357.58	0.00	604.1	0.32
20.5	0.04	238.5	0.94	358.33	0.00	610.5	0.74
22.5	0.70	239	0.84	359.08	0.00	612.9	0.89
29.5	0.73	245.6	0.79	360	0.00	615.25	1.02
36	0.77	252.17	0.37	360.83	0.00		
37.5	0.80	253.4	0.31	366.58	0.00		
39.5	0.85	254.67	0.19	372.33	0.00		
42.5	0.87	256.25	0.10	385.92	0.00		
45.83	0.93	257.83	0.04	399.5	0.01		
46.6	0.93	258.67	0.02	410.5	0.01		
47.83	0.94	259.5	0.02	424.17	0.04		
54.6	0.97	260.83	0.01	426.92	0.09		
61.33	0.90	262.17	0.01	429.25	0.34		
65.33	0.92	263.17	0.01	431.58	0.58		
69.33	0.91	269.42	0.35	440.2	0.77		
71.83	0.92	276.67	1.11	448.83	0.90		
79.3	0.92	277.9	1.20	451.67	0.97		
86.75	0.80	279.08	1.03	454.5	0.96		
100.83	0.81	280.33	1.21	461.9	0.69		
117.92	0.90	295.92	1.22	469.25	0.75		
118.25	0.82	298.4	1.18	470.9	0.80		
119	0.87	300.1	1.25	472.5	0.73		
132	0.89	301.83	1.24	475.1	0.87		
141.83	0.88	303.25	1.27	477.75	0.89		
142.33	0.90	304.67	1.23	486	0.71		
150	0.96	306	1.23	494.33	0.69		
155.17	0.93	307.42	1.10	503.83	0.91		
156.75	0.85	308.67	0.93	513.33	0.99		
159.33	0.55	317	0.83	518.5	1.05		
162.67	0.31	323.67	0.86	523.58	0.99		
164.5	0.58	325.2	0.90	524.7	1.01		
166.33	0.83	326.75	0.89	525.75	0.93		
175.25	0.97	328.33	0.91	535.3	1.00		
184.16	0.90	329.92	0.92	544.83	1.03		
187.3	1.00	331	0.84	546.4	1.06		
190.41	1.00	332.56	0.87	547.9	1.01		
199.41	0.82	334.83	0.88	549.6	1.05		
208.41	0.87	340	0.40	551.4	0.98		
211.08	0.79	345.25	0.03	560.25	1.07		
213.75	0.86	347.08	0.01	569.08	1.03		
222.92	0.85	348.92	0.02	571.5	0.72		
232.08	0.86	350.83	0.01	573.83	0.30		
233.08	0.89	352.75	0.01	583	0.05		
234.08	0.87	353.9	0.00	592.16	0.02		
237.33	0.93	355	0.00	595	0.01		

Table C.8. Zn C/C_0 values in the column effluent

time (h)	C/C_0
440.2	0.02
448.83	0.02
451.67	0.02
454.5	0.02
461.9	0.18
469.25	0.22
470.9	0.31
472.5	0.27
475.1	0.28
477.75	0.29
486	0.36
494.33	0.30
503.83	0.30
513.33	0.32
518.5	0.34
523.58	0.38
524.7	0.33
525.75	0.32
535.3	0.32
544.83	0.35
546.4	0.34
547.9	0.35
549.6	0.35
551.4	0.36
560.25	0.39
569.08	0.51
571.5	0.56
573.83	0.60
583	0.60
592.16	0.62
595	0.60
597.75	0.63
604.1	0.51
610.5	0.42
612.9	0.43
615.25	0.46

Table C.9. XRF concentrations of Mn and Zn in the column at the end of the experiment

height above column base	**Mn ($mg\ kg^{-1}$)**	**Zn ($mg\ kg^{-1}$)**
118-122 cm	212.9	8.2
115-118 cm	87.3	2.9
113-115 cm	39.1	2
100-113 cm	21.7	1.8
88-100 cm	17.9	1.6
75-88 cm	10.6	1.8
63-75 cm	8.7	1.4
50-63 cm	8.2	1.6
38-50 cm	7.9	1.4
25-35 cm	8.7	1.3
13-25 cm	8.8	1.3
0-13 cm	9.2	1.2
unreacted sand	6.3	1.5